Catalysis Science & Technology

Accepted Manuscript

ROYAL SOCIETY OF CHEMISTRY

www.rsc.org/catalysis

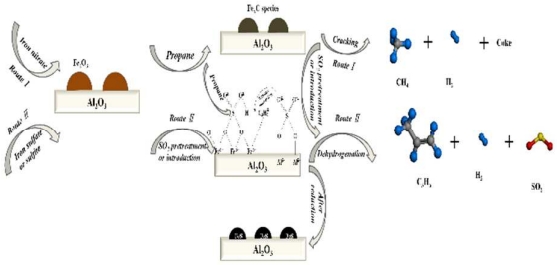

Highlights: The nature of the effect of sulfate species on properties and dehydrogenation performance of Fe_2O_3/Al_2O_3 catalysts were systematically studied.

Catalysis Science & Technology RSCPublishing

ARTICLE

Studies on the promoting effect of sulfate species in catalytic dehydrogenation of propane over Fe_2O_3/Al_2O_3 catalysts

Yanan Sun, Yimin Wu, Honghong Shan, Guowei Wang and Chunyi Li *

The promoting effect of sulfate species in propane dehydrogenation over Fe_2O_3/γ-Al_2O_3 catalysts is systematically elucidated by using iron (III) or iron (II) sulfate as the precursor, pre-treating with SO_2 or introducing SO_2 with propane as the reactant. At 560 °C, up to 23 wt% propylene yield with 80% selectivity is obtained. It is demonstrated that the introduced sulfate species exist in the form of SO_4^{2-} and strongly interact with the support and Fe via Al-O-S bond and Fe-O-S bond. On one hand, it suppresses the formation of Fe_xC species and thus the cracking reaction. On the other hand, it leads to an enhanced adsorption capacity of propane, meanwhile, the initial C-H bond activation and subsequent rupture with the formation of Fe-C_3H_7 and OH are facilitated, resulting in excellent dehydrogenation performance. On-line MS, XPS, XRD and reaction-regeneration-sulfuration results show that the loss of sulfate species by the reduction to S^{2-} and release in the form of SO_2 is the main reason for the deactivation of the sulfated catalysts.

1. Introduction

By virtue of the application in a number of important reactions including ethylbenzene dehydrogenation [1, 2], oxidative dehydrogenation of propane (ODHP) [3, 4] and F-T synthesis [5, 6], Fe-containing catalysts are amongst the most widespread catalytic systems in use today. However, despite years of intensive studies, the selectivity of propylene in ODHP remains low because of the strong side reactions such as oxidation and cracking reactions.

Compared with ODH, catalytic dehydrogenation of propane provides a more selective route to produce propylene using cheaper and abundant propane as the feedstock. Over the past few decades, most studies were focused on Cr-based [7-11] and Pt-based catalysts [12-16]. Though the activity and stability were greatly improved by either introducing alkali metals as the promoter or adopting new materials as the support, problems still exist, for instance, the serious environmental pollution of Cr-based catalysts and the high cost of Pt-based catalysts. Thus, developing a new cheap and environment-friendly catalytic system is of great importance.

In a previous paper [17], we reported the development of sulfated alumina supported iron catalysts as highly active and selective catalysts for catalytic dehydrogenation of propane, exhibiting propylene yield up to 20 wt% with 80% selectivity. An overview of characterization results revealed that SO_4^{2-} generated from sulfation of support significantly enhanced propane dehydrogenation by enhancing the acidity of the catalyst and the adsorption capacity of propane [17]. Nevertheless, aspects of the complex interaction between Fe_2O_3/Al_2O_3 catalyst and sulfate species, in particular the role of sulfate species in modifying the catalytic performance of Fe_2O_3/Al_2O_3 catalyst are still not clear.

The present work is complementary to the study of sulfated Fe_2O_3/Al_2O_3 catalysts and aims to gain insight into the origin of the promoting effect of sulfate species in propane dehydrogenation. First, the reaction was conducted over Fe_2O_3/γ-Al_2O_3 catalysts using iron (III) or iron (II) sulfate as the precursor, pre-treating with SO_2 or introducing SO_2 with propane in the reactant. Subsequently, the effects of sulfate addition on the structure, reducibility, acidity and adsorption-desorption behavior were discussed. Finally, a model was presented to interpret the promoting effect involving the build-up of

State Key Laboratory of Heavy Oil Processing, China University of Petroleum (East China), Qingdao 266580, P.R. China. E-mail addresses: chyli_upc@126.com, chyli@upc.edu.cn

Tel.: +86 532 86981862

Electronic Supplementary Information (ESI) available: MS signals of CO_2 and CO over 20FeAl-N catalyst, IR spectra of 20FeAl catalysts with different precursor, H_2-TPR profiles of 20FeAl catalysts with different precursor, Py-FT-IR spectra of 20FeAl-N, 20FeAl-560-SO_2 and 20FeAl-SA (II), reaction results over 20FeSi-SA (II), 20FeZr-SA (II) and pure Al_2O_3 in the reactant consisting of N_2, SO_2 and C_3H_8 at a molar ratio of 19:1:30, Al 2p spectra of unsulfated and sulfated Fe_2O_3/Al_2O_3 catalysts, reaction results over 20FeAl-N after reaction for 3 h and then treated with SO_2 or introduced SO_2 in the reactant, MS signal of CO_2 during the reaction-regeneration cycles over 20FeAl-SA (II) catalyst, reaction results in the reaction-regeneration-sulfuration cycles of 20FeAl-N, reaction results of the blank experiment as well as the reaction over pure Al_2O_3, SO_2-TG results at different temperature, The areas of reduction peaks quantified by peak deconvolution for sulfated and unsulfated catalysts, S 2p peak fitting calculation and analytical data of surface content of sulfated catalysts, textural properties of fresh, reacted, regenerated 20FeAl-SA (II) and 20FeAl-560-SO_2.

sulfate species, the corresponding reaction route over untreated and sulfated Fe_2O_3/Al_2O_3 catalysts was also proposed. Based on these results, it is hopeful to develop a new catalytic system involving sulfate for catalytic dehydrogenation of propane.

2. Experimental

2.1 Catalyst preparation

In our experiments, Fe_2O_3/Al_2O_3 catalysts (20 wt% loading of Fe_2O_3) were prepared by wet impregnation method using iron nitrate ($Fe(NO_3)_3 \cdot 9H_2O$, 99.9% purity), iron (III) sulfate ($Fe_2(SO_4)_3$, 99.9% purity) and iron (II) sulfate ($FeSO_4 \cdot 7H_2O$, 99.9% purity) as the precursor. After that, they were dried at 120 °C for 4 hours and calcined at 700 °C for 2 h. The obtained samples were denoted as 20FeAl-N, 20FeAl-SA (III), 20FeAl-SA (II) respectively.

2.2 Catalyst characterization

XRD patterns were obtained on a Rigaku D/Max RB diffractometer operated at 40 kV and 40 mA, using Cu Kα radiation with a scanning speed of 10 °/min.

FT-IR spectra were determined on Nicolet Nexus Fourier transform instrument. The background spectrum and the infrared spectrum of chemisorbed pyridine were recorded at 200 °C.

XPS studies were conducted using an ESCALab250 electron spectrometer from Thermo Scientific Corporation with monochromatic 150 W Al Ka radiation. The binding energy measurement was referenced to Al (2p) at 74.7 eV.

Temperature-programmed reduction experiment (H_2-TPR) was carried out in following procedures: 0.1 g catalyst of 0.3-0.9 mm diameter was heated under helium flow (30 mL/min) from room temperature to 200 °C and maintained for 1 h. After cooling down to 80 °C, the gas was switched to 10 vol%H_2/N_2 (30 mL/min) until the TCD signal being stable. Then the temperature was increased from 80 °C to 800 °C at a heating rate of 10°C/min.

SO_2 adsorption experiment of 20FeAl-N was performed on DTU-2A differential thermogravimetric analyzer. Temperature was first raised from 20 °C to the investigated temperature (450, 560, 600 °C) at a rate of 10 °C/min under the high purity nitrogen. Then SO_2 was introduced at a flow rate of 30mL/min for 90 min. Besides, the experiments over pure Al_2O_3 and Fe_2O_3 were also carried out at 700 °C.

C_3H_8 pulse adsorption-desorption experiment was carried out on the chemical adsorption apparatus with on-line MS analysis of effluent in following procedures. First, 0.1 g catalyst of 0.3-0.9 mm diameter was heated under helium flow (60 mL/min) from room temperature to 450 °C and maintained for 2 h to remove the adsorbed water, then cooled down to 150 °C. The MS signals of Ar (40), C_3H_8 (29) and He (4) were recorded until being constant. After that, the four-way valve was switched from He to Ar and C_3H_8 with the same flow rate (30 mL/min), after the signals no longer changed, switched to He again until the signal no longer changed, then switched to Ar and C_3H_8 and so forth. The same experiments were also conducted at 250 °C, 350 °C and 450 °C. For data processing, we select one pulse, fix the length of time and get the relative time value taking the starting time as the base (labeled as 0), then normalize the signal of Ar and C_3H_8 as follows: $\text{Intensity}=\frac{\text{The signal value}-\text{The minimum signal velue}}{\text{The maximum signal velue}}$. Finally, plot the normalize value of Intensity of Ar and C_3H_8 as the relative time, the area of the hysteresis loop represents the adsorbed capacity of propane. On-line MS analysis was conducted on the same apparatus, and the mass numbers of 18, 34, 64, and 43 were detected for H_2O, H_2S, SO_2 and C_3H_8.

2.3 Catalyst test

Catalytic dehydrogenation of propane was performed in a fixed-bed reactor (14mm in diameter) at 560 °C and under atmospheric pressure. In each experiment, 2 g of catalysts with the particle size of 0.088-0.180 mm were loaded in the middle of the reactor. Prior to reaction, the catalysts were pre-treated by nitrogen to remove adsorbed water. Then the reactant consisting of 99 wt% propane was introduced into the reactor at a flow rate of 12 mL/min. The product was analyzed by Bruker GC-450 chromatography.

The influence of SO_2 pre-treatment was investigated in the following procedures. The catalysts were firstly heated to the investigated temperatures (450 °C, 560 °C, 600 °C) in the atmosphere of nitrogen. Then 5 vol%SO_2/N_2 at a flow rate of 30 mL/min was introduced for 2 h. After that, switched to nitrogen and purged the reactor for 0.5 h to remove the residual SO_2. The effect of SO_2 was also studied by introducing 5 vol%SO_2/N_2 at a flow rate of 10 mL/min with propane as the reactant, that is, the reactant consists of N_2, SO_2 and C_3H_8 at a molar ratio of 19:1:24. The dehydrogenation performance of all catalysts was evaluated at the same reaction conditions: T=560 °C, P=1 atm, F_{C3H8}=12 mL/min.

The reaction-regeneration cycles over 20FeAl-SA (II) was performed on the chemical adsorption apparatus with on-line analysis of the product in following procedures. 0.1 g of catalyst with particle size of 0.3-0.9 mm was firstly heated to 560 °C at a heating ramp of 10 °C/min under helium flow (30 mL/min). The reactant was introduced at a flow rate of 12 mL/min for 20 min, then switched to air (30 mL/min), raised the temperature to 700 °C at a heating ramp of about 30 °C/min and maintained for 15 min. After that, the temperature was cooled to 560 °C/min under helium flow within 10 minutes. The reactant was introduced and another cycle was carried out following above steps. The m/e ratios of 18, 34, 64, 44, 43 and 41 were used to analyze H_2O, H_2S, SO_2, CO_2, C_3H_8 and C_3H_6.

The reaction-regeneration cycles over 20FeAl-560-SO_2 (2 g of catalyst) were carried out as below: reacted at 560 °C for 6 h in the reactor, then regenerated under air atmosphere at 700 °C in the muffle furnace for 1 h (the heating ramp is 30 °C/min), after that, treated the catalyst with SO_2 at a flow rate of 30 mL/min in the reactor for 2 h, then the reactant at a flow rate of 12 mL/min was introduced for another 6 h and so forth.

3. Results and discussion

3.1 Effect of precursor

To our knowledge, most of the Fe_2O_3/Al_2O_3 catalysts studied so far have been prepared by impregnation of Al_2O_3 with iron nitrate as the precursor. In this section, iron (III) and iron (II) sulfate were also adopted as the precursor and their performance in propane dehydrogenation was studied at 560 °C (Fig. 1). For 20FeAl-N, propylene was the main product in the initial stage. Subsequently, propane conversion along with methane yield increased dramatically with TOS. After 1 h, most of propane was converted to methane without the formation of propylene, suggesting a transformation from dehydrogenation reaction to cracking reaction. Besides, a

certain amount of oxidation products CO_x was detected (Fig. S1) due to the oxidation by oxygen species of iron oxide, which is consistent with previous study [18]. With extended reaction time, the oxygen species were fast consumed as evidenced by the dramatically decreased amount of CO_x (Fig. S1). To exclude the contribution of homogeneous gas phase reactions on the formation of methane, the blank experiment (without catalyst) and the reaction over pure Al_2O_3 were also carried out (Table S1). Under the reaction conditions, only around 1.0 wt% propane conversion and 0.1 wt% methane yield were obtained, demonstrating that the formation of methane is caused by the activation of the catalyst.

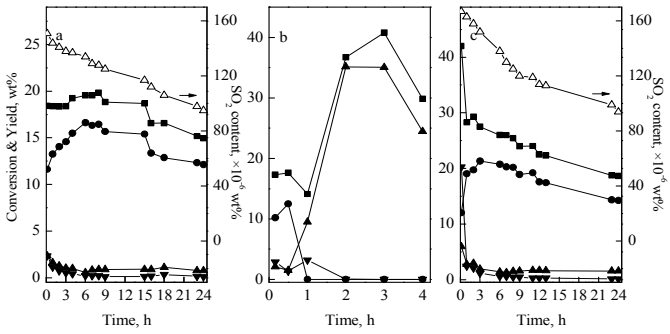

Fig. 1. Reaction results over (a) 20FeAl-SA (III), (b) 20FeAl-N, (c) 20FeAl-SA (II): (■) propane conversion; (●) propylene yield; (▲) methane yield; (▼) CO_x yield (Reaction conditions: T=560 °C, P=1 atm, F_{C3H8}=12 mL/min).

In comparison, 20FeAl-SA (III) and 20FeAl-SA (II) showed a completely different catalytic behavior in propane dehydrogenation. Propylene was the main product with much higher yield and selectivity. Moreover, higher amount of CO_x were observed, especially for 20FeAl-SA (II), 20 wt% CO_x yield (mainly CO_2) at an overall conversion of 42 wt% was obtained at TOS=15 min. After that, the yield of CO_x decreased dramatically. In addition to CO_x, methane was another main product other than propylene in the initial stage of the reaction. Since no oxidant was introduced during the reaction, it was speculated that surface oxygen species made a great contribution to the formation of CO_x and methane. Combining with the "induction period" of propylene yield over 20FeAl-SA (III) and 20FeAl-SA (II), it seems to suggest that iron species with low oxidation number play an important role in dehydrogenation reaction.

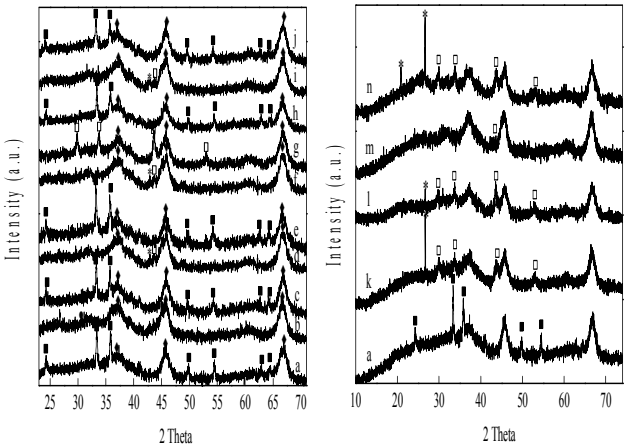

Fig. 2. XRD patterns of: (a) fresh 20FeAl-N, (b) 20FeAl-N after reaction for 2 h, (c) 20FeAl-SA (III), (d) 20FeAl-SA (III) after reaction for 24 h, (e) 20FeAl-SA (II), (f) 20FeAl-SA (II) after reaction for 3 h, (g) 20FeAl-SA (II) after reaction for 24 h; (h) fresh 20FeAl-560-SO_2; (i) 20FeAl-560-SO_2 after reaction for 6 h; (j) 20FeAl-560-SO_2 after four reaction-regeneration cycles; 20FeAl-N under reactant with a molar ratio of N_2: SO_2: C_3H_8=19:1:30 at (k) TOS=6 h; (l) TOS=14 h; 20FeAl-N catalyst after reaction for 3 h, then (m) under reactant with a molar ratio of N_2: SO_2: C_3H_8=19:1:30 at TOS=8 h; (n) treated with SO_2 and then reacted for 8 h: (■) Fe_2O_3, (●) Fe_xC, (□) FeS, (*) SiO_2, (◆) Al_2O_3.

In above experiments, it is found that 20FeAl-N catalyst produces abundant methane instead of propylene as the reaction proceeds, which is probably caused by the changes in iron species under the reducing dehydrogenation environment. To obtain more information about the changes in iron phase during the reaction, XRD characterization of 20FeAl-N reacted for 2 h, which showed high cracking activity and yielded most methane was conducted and shown in Fig. 2. After reaction for 2 h, characteristic peaks of Fe_2O_3 disappeared while that of metallic Fe or Fe_xC appeared, which are supposed to be active for C-C scission, especially through propane hydrogenolysis reaction [19]. Since the resolution of the XRD diffraction peaks is rather poor, XPS characterization of reacted 20FeAl-N was conducted (Fig. 5). After reaction for 2 h, Fe $2p_{3/2}$ peak at around 708.5 eV indicative of Fe_xC species appeared. Therefore, it is deduced that the Fe_xC species generated during the course of reaction facilitate the undesirable cracking reaction and hence the formation of methane. Compared with 20FeAl-N, only diffraction lines of FeS were detected for sulphated catalysts after reaction (Fig. 2), and the longer the reaction time, the stronger the intensity of FeS, as evidenced by the S 2p peak locates at around 162 eV (Fig. 8). Thus, the cracking reaction was greatly inhibited.

Moreover, propylene yield and selectivity increased dramatically with iron (III) and iron (II) sulfate as the precursor. One possible explanation would be the formation of sulphate. Nevertheless, all the catalysts only exhibited diffraction lines of Fe_2O_3 without any peak corresponding to iron sulphate or aluminium sulphate (Fig. 2), indicating that under the high calcination temperature (700 °C), iron (III) and iron (II) sulfate were completely decomposed to Fe_2O_3 with the release of sulfur oxides following the reactions:

$$2FeSO_4 \rightarrow Fe_2O_3 + SO_2 + SO_3 \quad (1)$$

$Fe_2(SO_4)_3 \rightarrow Fe_2O_3 + 3SO_3$ (2)

However, according to literatures [20, 21], SO_2 and SO_3 can adsorb on the surface of γ-Al_2O_3 and Fe_2O_3, giving rise to S–O–Al and S–O-Fe groups. To verify the speculation, SO_2 adsorption experiment was conducted and the results were tabulated in Table S2. It is obvious that apart from γ-Al_2O_3, Fe_2O_3 is also active in adsorbing SO_2 with 2.8 wt% weight gain rate at 700 °C. This can be attributed to the strong electron affinity of surface adsorbed oxygen (O^-) and lattice oxygen (O^{2-}) of Fe_2O_3, which makes it easy for SO_2 to adsorb on the surface or form complex. Furthermore, the IR spectra of 20FeAl-SA (III) and 20FeAl-SA (II) were characterized and shown in Fig. S2. The appearance of two obvious absorption bands at around 1390 and 1090 cm^{-1} confirms the formation of aluminum sulphate [20]. In addition, four absorption bands at 1190-1170, 1110-1130, 1035-1030, 990 cm^{-1} assigned to the asymmetric and symmetric frequencies of S-O bonds in SO_4^{2-} that coordinates to one or two iron ions through its oxygen were observed [21]. Based on these results, it is concluded that the generated SO_x further adsorbs on both alumina and Fe_2O_3, causing the formation of stable SO_4^{2-} species, which are supposed to contribute to the improved catalytic performance.

According to above results, it is speculated that the reduction of Fe_2O_3 to Fe_xC species is greatly inhibited in the presence of sulfate species. To verify above speculation, H_2-TPR characterization was performed and displayed in Fig. S3, the areas of reduction peaks for the catalysts quantified by peak deconvolution were listed in Table S3. As for 20FeAl-N, three reduction peaks attributing to the reduction of surface adsorbed oxygen species, the reduction process of $Fe_2O_3 \rightarrow Fe_3O_4$ and $Fe_3O_4 \rightarrow FeO + Fe$ [22-25] were observed. The shape of TPR patterns for 20FeAl-SA (III) and 20FeAl-SA (II) was very similar. However, peak 2 at around 450 °C showed a much larger area while peak 3 shifted to lower temperature (from 620 °C to 550 °C) with a smaller area. It is worth noting that a shoulder peak (peak 2') at about 400 °C was observed for 20FeAl-560-SO_2, which was ascribed to the reduction of sulfate species [26, 27]. Therefore, it is concluded that a larger amount of Fe^{3+} are much easier to be reduced to Fe^{2+}. Meanwhile, with the reduction from SO_4^{2-} to S^{2-}, FeS was produced at the expense of Fe_xC species, thus the generation of abundant methane were inhibited.

On the basis of above results, it is believed that iron (III) and iron (II) sulfate are decomposed to Fe_2O_3 with the retention of sulfate species in the process of calcination, which suppresses the reduction from iron oxide to Fe_xC species and consequently the cracking reaction, furthermore, the dehydrogenation reaction is greatly improved.

3.2 Effect of SO_2 pretreatment and introduction in the reactant

To confirm the promoting effect of sulfate species in propane dehydrogenation, 20FeAl-N was pre-treated with SO_2 before reaction under different temperatures (450 °C, 560 °C, 600 °C) as described in section 2.3, the obtained samples were referred to as 20FeAl-x-SO_2 (x represents the treating temperature) and performed in propane dehydrogenation (Fig .3). Likewise, SO_2 pretreatment dramatically inhibited the formation of methane, and the lower the temperature, the higher the dehydrogenation activity. With increased reaction time, propane conversion and propylene yield all decreased with a diminishing content of SO_2 in the product, which is consistent with aforementioned results.

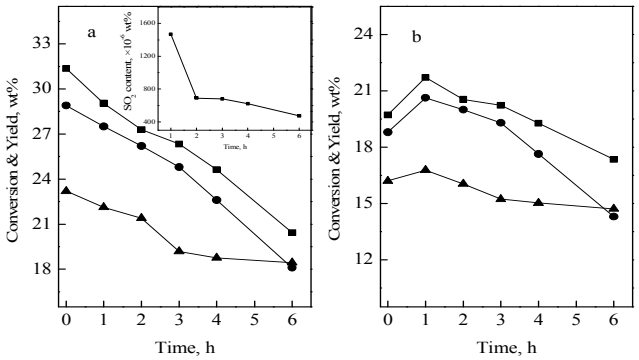

Fig. 3. Effect of SO_2 pre-treatment temperature on propane conversion (a) and propylene yield (b) over 20FeAl-N catalyst: (■) 450 °C; (●) 560 °C; (▲) 600 °C (Reaction conditions: T=560 °C, P=1 atm, F_{C3H8}=12 mL/min).

Among studies on propane dehydrogenation published up to now, the effect of sulfate species has not been clearly defined. In a previous paper [28], Wang et al. found that addition of sulfate species improved the performance of Cr_2O_3/SiO_2 catalyst in ethane dehydrogenation and attributed the increased activity to enhanced acidity. In this regard, the present results are in perfect agreement. As shown in Fig. S4, the FT-IR spectrum of 20FeAl-N only exhibited an adsorption band at 1450 cm^{-1} attributed to the chemisorption of pyridine on Lewis acid sites [29-32]. The introduction of sulfate species led to the formation of Bronsted acid sites. Therefore, it is deduced that the strengthened acidity caused by the sulfate species is responsible for the excellent catalytic performance.

To sum up, the improved acidity and reducibility of sulfated 20FeAl catalysts is considered to be related to the existence of sulfate species [17]. Due to the strong electron-withdrawing ability of sulfate ion, the neighboring iron ion is more electropositive, in which case Fe-O-S bond is strengthened [33, 34]. On the other hand, the strong interaction between iron cations and oxygen species frees a hydrogen proton of the coordinated water, which generates Bronsted acid sites [35] and enhances the dehydrogenation activity.

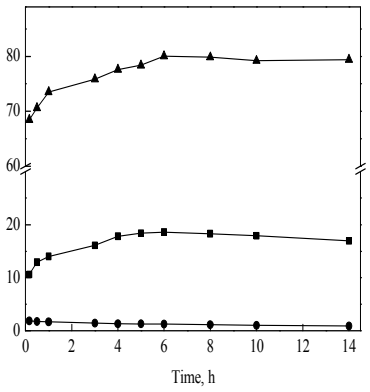

Fig. 4. Effect of SO_2 introduction on the performance of 20FeAl-N catalyst: (■) propylene yield; (●) methane yield; (▲) selectivity of propylene (Reaction conditions: T=560 °C, P=1 atm, F_{C3H8}=12 mL/min).

To further authenticate the important role of sulphate species in propane dehydrogenation, 5 vol%SO_2/N_2 was introduced with C_3H_8 as the reactant, and the molar ratio of N_2: SO_2: C_3H_8 was 19:1:30 (Fig. 4). During the investigated 14 h, most of propane was converted to propylene with about 80% selectivity and 20 wt% yield, which can be ascribed to the formation of sulfate species caused by the strong adsorption capacity of SO_2 on the catalyst. However, under the dehydrogenation atmosphere, the sulfate species were also reduced to FeS as detected by XRD technique (Fig. 2).

All in all, the introduction of sulfate species to Fe_2O_3/Al_2O_3 catalysts either by using iron (III) and iron (II) sulfate as the precursor, pretreating with SO_2 or introducing SO_2 with C_3H_8 as the reactant significantly alters the course of reaction, turning propane dehydrogenation into the predominant reaction. In view of the excellent activity and selectivity, the greatly improved dehydrogenation performance is related to the sulfate species formed by adsorption of SO_x. Detailed elaboration will be found in following sections.

3.3 The nature of the effect of sulfate species on the catalytic performance of Fe_2O_3/Al_2O_3 catalyst

As for heterogeneous catalytic reactions, the adsorption of reactant exerts an important impact on the catalytic behaviour. To get a deeper insight into the nature of the effect of sulfate species on the properties and catalytic performance of Fe_2O_3/Al_2O_3 catalyst, XPS characterization and C_3H_8 adsorption-desorption experiment were firstly carried out and corresponding results were displayed in Fig. 5 and Fig. 6.

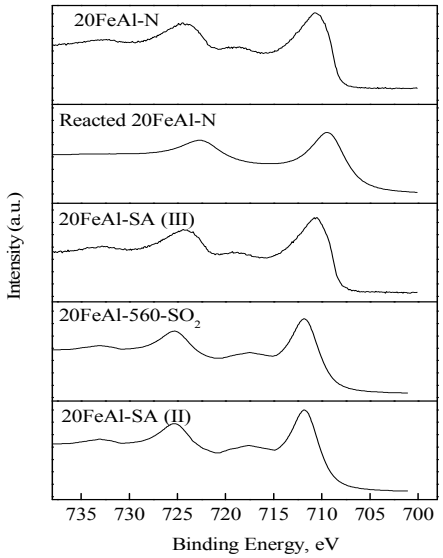

Fig. 5. Fe 2p peaks of unsulfated, sulfated Fe_2O_3/Al_2O_3 catalysts and 20FeAl-N reacted for 2 h.

All the fresh samples showed Fe $2p_{3/2}$ peak between 710.6 and 711.5 eV with its associated 3d→4s satellite peak at 718.7 eV, indicating that Fe species are characteristic of Fe^{3+} in Fe_2O_3 as proved by the spin-orbital splitting of around 13.5 eV between Fe $2p_{3/2}$ and Fe $2p_{1/2}$ peaks [36-38]. After sulfate addition, the band position shifted to higher binding energy, which can be ascribed to the strong electron-withdrawing ability of sulfate species, causing an electron transfer from Fe to S and the formation of Fe species at electron-deficient state.

In the process of propane dehydrogenation, it is widely accepted that the initial adsorption of propane on the active sites and subsequent rupture of C-H bond plays the key role in the formation of propylene [39-42]. In view of the significantly meliorated catalytic performance, C_3H_8 pulse adsorption-desorption was carried out as described in section 2.2 and the results were depicted in Fig. 6. Compared with 20FeAl-N, the adsorption capacity of propane (proportional to the area of hysteresis loop) increased dramatically for sulfated catalysts. Since the secondary carbon of propane has 0.051 negative charges, they are more likely to adsorb, which is in favor of the reaction [43].

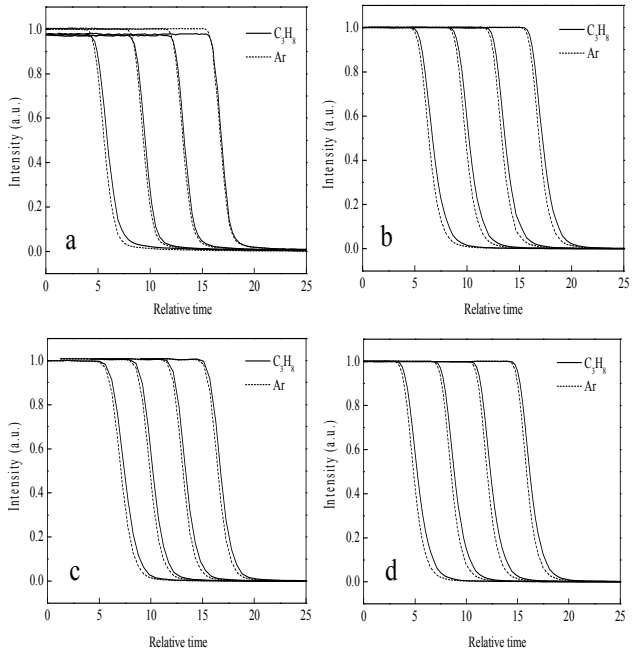

Fig. 6. C_3H_8 pulse adsorption-desorption isotherms over (a) 20FeAl-N; (b) 20Fe/S-Al; (c) 20FeAl-SO_2-560; (d) 20FeAl-SA (II).

From foregoing results, it can be concluded that sulfate addition to Fe_2O_3/Al_2O_3 catalysts improves the electronic property, leading to enhanced acidity and adsorption capacity of propane. According to the results in section 3.1, SO_x can adsorb on both Al_2O_3 and Fe_2O_3, resulting in the generation of sulphate species. To get more knowledge about the nature of the effect of sulphate species, the reaction was performed over 20FeSi-SA (II), 20FeZr-SA (II) catalysts under the same reaction conditions and pure Al_2O_3 in the reactant consisting of N_2, SO_2 and C_3H_8 at a molar ratio of 19:1:30 (Fig. S5). Both activity and stability decreased dramatically with SiO_2 and ZrO_2 as the support, especially over 20FeSi-SA (II), only 6.1 wt% propylene yield was achieved, proving the important role of Al_2O_3. However, pure Al_2O_3 exhibited very lower activity (about 4 wt% propylene yield), suggesting that the existence of Fe_2O_3 is indispensable for the improved catalytic performance.

Based on above results, it is inferred that in spite of low reactivity, the existence of alumina support enhances the adsorption capacity of SO_x, hence the formation and reservation of sulphate species, which contributes to the higher stability. This was further verified by the

higher binding energy of Al 2p spectra of sulphated catalysts (Fig. S6), which indicates an electron transfer from Al to S in the structure of Al-O-S groups. Therefore, we put forward a model for the promoting effect of sulfate species in a manner similar to that proposed by Choudhary and Rane [44] for methane activation over oxide catalysts and that proposed by Burch et al. [45, 46] for propane activation over Pt/Al_2O_3 catalysts (Scheme 1). In this model, the alumina support facilitates the formation of the electronegative sulfate groups, which are believed to involve in the reaction. When propane is adsorbed on the catalyst, H atoms are abstracted from propane by its polarization followed by C-H bond rupture to form $C_3H_7^+$ and H^-, which will interact with $Fe_{LC}^{\delta+}$ and $O^{\delta-}$ (LC denotes low coordination) respectively. According to this mechanism, the lower coordinated Fe sites are in favor of propane dehydrogenation, agreeing with the observed "induction period" for propylene yield over sulphated catalysts.

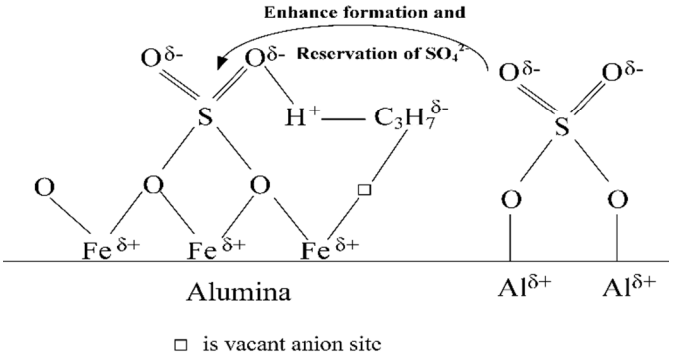

Scheme 1. Proposed model for the promoting effect of sulfate species on propane dehydrogenation over Fe_2O_3/Al_2O_3 catalysts.

In order to further validate the promoting effect of sulfate species, SO_2 was introduced likewise to 20FeAl-N catalyst after reaction for 3 h, which showed high cracking activity (Fig. S7). Similarly, both introducing SO_2 with propane in the reactant and treating with SO_2 brought about much higher yield and selectivity of propylene. During the first 1 h of the introduction of SO_2, methane was still the main product, after 3 h, the yield of propylene increased from 3 wt% to 25 wt%. Whereas after treating with SO_2, propane became the dominant product with yield up to 23 wt%. Besides, FeS was detected after reaction (Fig. 2), suggesting that SO_2 can also directly interact with Fe_xC species, leading to the formation of sulfate species and thus promoting dehydrogenation reaction.

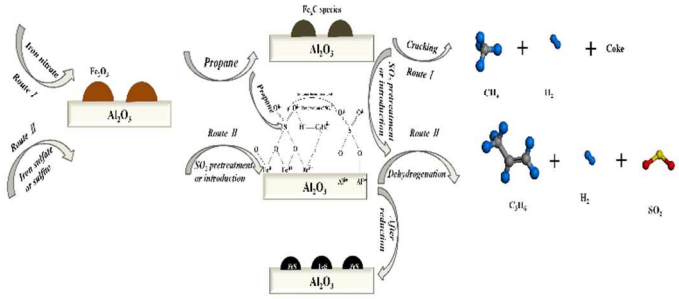

Scheme 2. Effect of sulfate addition on the reaction route of propane over 20FeAl catalyst.

On the basis of above results and discussions, the course of reaction over unsulfated and sulfated 20FeAl catalysts is proposed and depicted in Scheme 2. In the absence of sulfate species, propane is first dehydrogenated to propylene over iron oxide. Simultaneously, Fe_2O_3 is reduced to Fe_xC species which constitute the active sites for cracking reaction (Route I), hence resulting in the formation of abundant methane. When sulfate species are introduced either from the beginning of the reaction or after reaction with the formation of large amount of methane, they strongly interact with the support and Fe^{n+} via Al-O-S bond and Fe-O-S bond. In this model, the initial C-H bond activation and subsequent rupture are facilitated due to the modified electronic property caused by the strong electron-withdrawing ability of SO_4^{2-}. For another, the generation of Fe_xC species is suppressed due to the formation of FeS, thus inhibiting cracking reaction. Nevertheless, concerning the essence of the dramatically improved catalytic behavior by sulfate species, detailed work about the adsorption state, the possible adsorbed intermediate species still needs to be carried out.

3.4 Origin of catalyst deactivation

Although the buildup of sulfate species dramatically improves the performance of Fe_2O_3/Al_2O_3 catalysts, the activity gradually declines with prolonged reaction time As indicated in Fig. 2, FeS was generated at the expense of Fe_2O_3 after reaction for sulfated catalysts, and the longer the reaction time, the stronger intensity of diffraction lines of FeS, suggesting a reduction process of Fe^{3+} and SO_4^{2-}, which is supposed to be responsible for the catalyst deactivation.

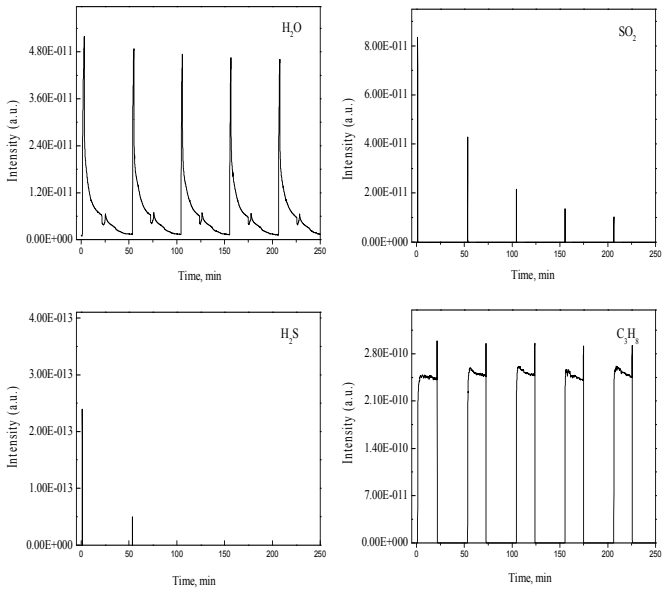

Fig. 7. MS spectra from the reaction-regeneration cycles over 20FeAl-SA (II) catalyst.

Fig. 7 exhibited the MS spectra from the reaction-regeneration experiment (as described in section 2.3) over 20FeAl-SA (II) catalyst. Within the investigated cycles, SO_2 and H_2S (with a much weaker intensity) were detected at the same time, which was ascribed to the reduction of sulfate groups [47]. As the number of cycles increased, the concentration of SO_2, H_2S and H_2O declined dramatically while that of C_3H_8 showed an increasing trend, all of

which point to the fact that sulfate groups are reduced and released in the form of SO_2 during the reaction, constituting the reason for the deactivation of the catalyst. In addition, an increasing amount of CO_2 (Fig. S8) was detected during the process of regeneration, suggesting that with the consumption of sulphate species, more and more carbon deposition was generated, which also contributes to the declined dehydrogenation activity.

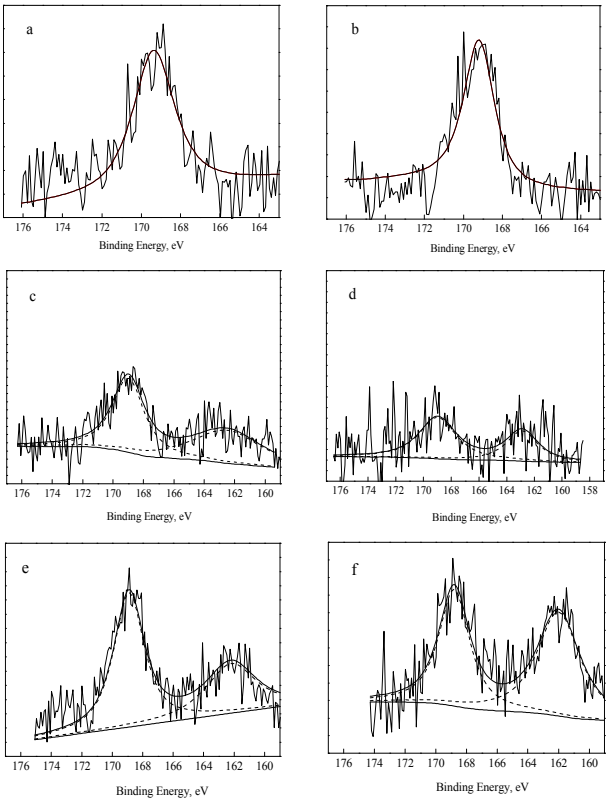

Fig. 8. S 2p spectra of (a) 20FeAl-560-SO_2; (b) 20FeAl-SA (II); (c) 20FeAl-SA (II) after reaction for 3 h; (d) 20FeAl-SA (II) after reaction for 24 h; (e) 20FeAl-SA (III) after reaction for 24 h; (f) 20FeAl-560-SO_2 after reaction for 6 h.

To get more information about the nature and number of sulfur species, S 2p spectra of fresh and reacted sulphated catalysts were characterized and depicted in Fig. 8. The samples pre-treated with SO_2 or adopting iron (II) sulfate as the precursor exhibited S 2p peak located at 169.8 eV assigned to S-O bond in SO_4^{2-} [36], which is in good accordance with IR results in Fig. S2. After reaction for 3 h, 20FeAl-SA (II) showed two peaks at around 168.5 eV and 162.4 eV, which are attributed to SO_3^{2-} and S^{2-} in FeS. After 24 h, the percentage area of S^{2-} further increased (Table S4), verifying the reduction process from SO_4^{2-} to S^{2-} during the course of reaction. Similar results were found over 20FeAl-SA (III) and 20FeAl-560-SO_2 after reaction. Combining with the results in section 3.3, it is concluded that both sulfate groups and iron species play an important role in the reaction. The loss of sulfate groups in the form of SO_2 and the reduction to FeS are the main reasons for the deactivation of sulfated catalysts.

In order to recover the activity, 20FeAl-N was treated with SO_2 for another 2 h after every 6 h of reaction, totally four such reaction-regeneration-sulfuration cycles were carried out. As shown in Fig. S9, the activity was largely restored after the sulfuration treatment, further demonstrating that the existence of sulfate species is essential to the excellent dehydrogenation performance and its loss causes the deactivation of the catalyst.

As far as we know, the best catalysts in propane dehydrogenation were commercial Cr-based and Pt-based catalysts, eg: 44% propylene yield with 87% selectivity were obtained at 650 °C, 0.05 MPa over Cr-based catalysts, while 40% propylene yield with 84% selectivity are obtained at 525 °C and 0.2 MPa over Pt-based catalysts. Though the activity (23 wt% propylene yield with 80% selectivity) of sulfated catalysts is lower, it is more environment-friendly compared with Cr-based catalysts and cheaper than Pt-based catalysts.

Besides, it is widely accepted that with increased number of regeneration, the entrapment and migration of Cr species into the support [42, 48] and the sintering of Pt particles [49, 50] causes the irreversible deactivation of the catalysts. In comparison, the activity of the catalyst can be largely recovered after regeneration and sulfuration treatment (Fig. S9). What's more, as tabulated in Table S5, despite the surface area of 20FeAl-560-SO_2 diminished after reaction, eg: decreased from 149.1 m^2/g to 140.8 m^2/g and 136.9 m^2/g after reaction in the first and fourth cycle, it increased to 145.8 m^2/g and 142.2 m^2/g again after regeneration. Similar results were found over 20FeAl-SA (II). XRD results also showed that after the fourth regeneration, Fe_2O_3 with slightly reduced intensity was observed over 20FeAl-560-SO_2, all of which suggested that the sulfated iron catalysts have a more stable structure, making them a kind of promising catalytic system for catalytic dehydrogenation of propane.

4. Conclusions

The promoting effect of sulfate species on the performance of Fe_2O_3/Al_2O_3 catalyst in propane dehydrogenation was studied by using iron (II) or iron (III) sulfate as the precursor, pre-treating with SO_2, introducing SO_2 with propane in the reactant either from the beginning of the reaction or during the reaction when most propane was converted to methane. In the presence of sulfate species, propane dehydrogenation becomes the dominant reaction with propylene yield up to above 20 wt% and selectivity to 80%.

It is found that on one hand, sulfate addition inhibits the formation of Fe_xC species during the course of reaction, hence inhibiting cracking reaction and the formation of methane. On the other hand, the introduced sulfate species exist in the form of SO_4^{2-} and interact strongly with the support and Fe species via Al-O-S and Fe-O-S bond, in which structure the initial C-H bond activation and rupture are facilitated by the electronegative sulfate sites and iron species at low coordination number, all of which are beneficial for the formation of propylene.

Concerning the catalyst deactivation, on-line MS, XPS and XRD results show that the loss of sulfate species caused by the reduction to S^{2-} or release in the form of SO_2 is the main reason for the deactivation. After sulfuration treatment with SO_2 after regeneration of the catalyst, the activity could be largely restored, verifying the key role of sulfate species in the significantly improved dehydrogenation performance.

Acknowledgements

This work is supported by National Natural Science Foundation of China (Grant No.U1362201) and the Fundamental Research Funds for the Central Universities (No. R1404019A).

Notes and references

1 M. Muhler, J. Schutze, M. Wesemann, T. Rayment, A. Dent, R. Schlogl, G. Ertl, J. Catal. 1990, 126, 339.

2 W.P. Addiego, C.A. Estrada, D.W. Goodman, M.P. Rosynek, R.G. Windham, J. Catal. 1994, 146, 407.

3 E.V. Kondratento, J. Perez-Ramirez, Appl. Catal. A 2004, 267, 181.

4 R. Bulanek, B. Wichterlova, K. Novoveska, V. Kreibich, Appl. Catal. A 2004, 264, 13.

5 H.M.T. Galvis, A.C.J. Koeken, J.H. Bitter, T. Davidian, M. Ruitenbeek, A.I. Dugulan, K.P. de Jong, J. Catal. 2013, 303, 22.

6 L.A. Cano, M.V. Cagnoli, J.F. Bengoa, A.M. Alvarez, S.G. Marchetti, J. Catal. 2011, 278, 310.

7 F. Cabrera, D. Ardissone, O.F. Gorriz, Catal. Today 2008, 133, 800.

8 Ch. Marcilly, B. Delmon, J. Catal. 1972, 24, 336.

9 D.S. Kim, I.E. Wachs, J. Catal. 1993, 142, 166.

10 F. Cavani, M. Koutyrev, F. Trifiro, A. Bartolini, D. Ghisletti, R. Lezzi, A. Santucci, G. Del Piero, J. Catal. 1996, 158, 236.

11 E. Rombi, M.G. Cutrufello, V. Solinas, S. De Rossi, G. Ferraris, A. Pistone, Appl. Catal. A 2003, 251, 255.

12 S.B. Zhang, Y.M. Zhou, Y.W. Zhang, L. Huang, Catal. Lett. 135 2010, 135, 76.

13 E.L. Jablonski, A.A. Castro, O.A. Scelza, S.R. Miguel, Appl. Catal. A 1999, 183, 189.

14 P.P. Sun, G. Siddiqi, M.F. Chi, A.T. Bell, J. Catal. 2010, 274, 192.

15 D. Akporiaye, S.F. Jensen, U. Olsbye, F. Rohr, E. Rytter, M. Rønnekleiv, A.I. Spjelkavik, Ind. Eng. Chem. Res. 2001, 40, 4741.

16 P.P. Sun, G. Siddiqi, W.C. Vining, M.F. Chi, A.T. Bell, J. Catal. 2011, 282, 165.

17 Y.N. Sun, L. Tao, T.Zh. You, Ch.Y. Li, H.H. Shan, Chem. Eng. J. 2014, 244, 145.

18 R.J. Li, S.K. Shen, J. Mol. Catal. (China) 2001, 15, 181.

19 C.J. Machiels, R.B. Anderson, J. Catal. 1979, 58, 253.

20 C.C. Chang, J. Catal. 1978, 53, 374.

21 T. Yamaguchi, T. Jin, K. Tanabe, J. Phys. Chem. 1986, 90, 3148.

22 H.H. Dong, M.J. Xie, J. Xu, M.F. Li, L.M. Peng, X.F. Guo, W.P. Ding, Chem. Commun 2011, 47, 4019.

23 N.W. Hurst, S.J. Gentry, A. Jones, B.D. McNicol, Catal. Rev. Sci. Eng. 1982, 24, 233.

24 O.J. Wimmer, P.J. Arnoldy, J.A. Mouljin, J. Phys. Chem. 90 1986, 90, 1331.

25 P. Michorczyk, P. Kustrowski, L. Chmielarz, J. Ogonowski, React. Kinet. Catal. Lett. 2004, 82, 121.

26 P.J. Magnus, A. Riezebos, A.D. van Langeveld, J.A. Mooljin, J. Catal. 1995, 151, 178.

27 K. Inamura, T. Takyu, K. Okamoto, K. Nagata, T. Imanaka, J. Catal. 1992, 133, 498.

28 Sh.B. Wang, K. Murata, T. Hayakawa, S. Hamakawa, K. Suzuki, Catal. Lett. 1999, 63, 59.

29 M.C. Abello, M.F. Gomez, L.E. Cadus, Catal. Lett. 1998, 53, 185.

30 K.D. Chen, S. Xie, A.T. Bell, J. Catal. 2000, 195, 244.

31 A. Galli, J.M. Lopez-Nieto, Catal. Lett. 1995, 34, 51.

32 B.H. Li, R.D. Gonzalez, Catal. Today 1998, 46, 55.

33 J. Benziger, R. Madix, J. Surf. Sci. 1980, 94, 119.

34 T.J. Vink, L.L.J. Gijzeman, J.W. Geus, Surf. Sci. 1985, 150, 14.

35 Y.L. Gu, Sh.Zh. Liu, Ch.Y. Li, Q.K. Cui, J. Catal. 2013, 301, 93.

36 C.S. Kuivila, J.B. Butt, P.C. Stair, Appl. Surf. Sci. 1988, 32, 99.

37 D.B. Bukur, K. Okabe, M.P. Rosynek, C.P. Li, D.Y. Wang, K.R.P. M. Rao, G.P. Huffman, J. Catal. 1995, 155, 353.

38 T. Yamashita, P. Hayes, Appl. Surf. Sci. 2008, 254, 2441.

39 R. Burch, R. Swarnakar, Appl. Catal. 1991, 70, 129.

40 K.D. Chen, A. Khodakov, J. Yang, A.T. Bell, E. Iglesia, J. Catal. 1999, 186, 325.

41 K.D. Chen, E. Iglesia, A.T. Bell, J. Catal. 2000, 192, 197.

42 B.M. Weckhuysen, R.A. Schoonheydt, Catal. Today 1999, 51, 223.

43 H.C. Yao, H.K. Stepien, H.S. Gandhi, J. Catal. 1981, 67, 231.

44 V.R. Choudhary, V.H. Rane, J. Catal. 1991, 130, 411.

45 R. Burch, E. Halpin, M. Hayes, K. Ruth, J.A. Sullivan, Appl. Catal., B 1998, 19, 199.

46 A. Hinz, M. Skoglundh, E. Fridell, A. Andersson, J. Catal. 2001, 201, 247.

47 F. Cavani, S. Guidetti, C. Trevisanut, E. Ghegini, M. Signoretto, Appl. Catal. B 2010, 100, 197.

48 R.L. Puurunen, B.G. Beheydt, B.M. Weckhuysen, J. Catal. 2001, 204, 253.

49 R.M.J. Fiedorow, B.S. Chahar, S.E. Wanke, J. Catal. 1978, 51, 193.

50 J.A. Moulijn, A.E. van Diepen, F. Kapteijn, Appl. Catal. A 2001, 212, 3.